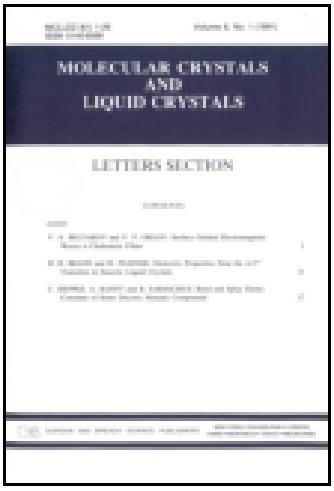

Molecular Crystals and Liquid Crystals
Publication details, including instructions for authors and subscription information:
http://www.tandfonline.com/loi/gmcl20

Thermal, Optical, and Dielectric Analysis of Hydrogen-Bonded Liquid Crystals Formed by Adipic and Alkyloxy Benzoic Acids

A. J. Gopunath[a], T. Chitravel[a], C. Kavitha[b], N. Pongali Sathya Prabu[b] & M. L. N. Madhu Mohan[b]

[a] University College of Engineering, Anna University, Ramanathapuram, Tamil Nadu, India

[b] Liquid Crystal Research Laboratory (LCRL), Bannari Amman Institute of Technology, Sathyamangalam, Tamil Nadu, India

Published online: 28 Apr 2014.

To cite this article: A. J. Gopunath, T. Chitravel, C. Kavitha, N. Pongali Sathya Prabu & M. L. N. Madhu Mohan (2014) Thermal, Optical, and Dielectric Analysis of Hydrogen-Bonded Liquid Crystals Formed by Adipic and Alkyloxy Benzoic Acids, Molecular Crystals and Liquid Crystals, 592:1, 63-81, DOI: 10.1080/15421406.2013.839315

To link to this article: http://dx.doi.org/10.1080/15421406.2013.839315

Mol. Cryst. Liq. Cryst., Vol. 592: pp. 63–81, 2014

ISSN: 1542-1406 print/1563-5287 online
DOI: 10.1080/15421406.2013.839315

Thermal, Optical, and Dielectric Analysis of Hydrogen-Bonded Liquid Crystals Formed by Adipic and Alkyloxy Benzoic Acids

A. J. GOPUNATH,[1] T. CHITRAVEL,[1] C. KAVITHA,[2]
N. PONGALI SATHYA PRABU,[2]
AND M. L. N. MADHU MOHAN[2,*]

[1]University College of Engineering, Anna University, Ramanathapuram, Tamil Nadu, India
[2]Liquid Crystal Research Laboratory (LCRL), Bannari Amman Institute of Technology, Sathyamangalam, Tamil Nadu, India

Intermolecular hydrogen-bonded homologous series comprising of eight liquid crystalline complexes are isolated and characterized. Double complimentary hydrogen bonds are formed between non-mesogen adipic acid (AA) and mesogenic p-n-alkyloxy benzoic acid (nBAO), the series is referred to as AA+nBAO. Hydrogen bond formation is evinced through Fourier transform infrared spectroscopy (FTIR) studies, while the mesogenic phases are identified by polarizing optical microscopic (POM) studies, which are further confirmed by differential scanning calorimetry (DSC). Phase diagram is constructed from the data of DSC and POM studies. The variation of tilt angle with temperature in smectic C phase is fitted to a power law and the exponent value (β) is found to be in agreement with Mean Field predicted value.

Keywords Dielectric hysteresis; dielectric relaxation; hydrogen-bonded liquid crystals; mean field; odd-even effect

1. Introduction

Technology boom aided with the usage of liquid crystal displays (LCDs) in the recent years scored the liquid crystalline materials to be implemented for different engineering device applications [1,2]. These technical developments made the liquid crystal scientists over the globe [3–7] to synthesize and characterize enormous mesogenic materials for display applications. Among the existing types of liquid crystals, hydrogen-bonded liquid crystals (HBLCs) play a pivotal role due to their thermal stability, high directionality and dynamics for chemical, and biological processes in nature. Various types of HBLCs, viz., single bond [8,9], double bond [10,11], and even multiple bonded [12,13] HBLCs formation have been reported earlier as it plays a key role in associating the molecules. The first ever-reported hydrogen-bonded complex exhibiting mesogenic nature is formed by the carboxylic acids [14]. The so-formed mesogenic complexes dimerize through intermolecular

*Address correspondence to M. L. N. Madhu Mohan, Liquid Crystal Research Laboratory (LCRL), Bannari Amman Institute of Technology, Sathyamangalam, Tamil Nadu 638 401, India, Tel: +91 9442437480; Fax: +91 4295 223 775. E-mail: mln.madhu@gmail.com

hydrogen bonding, which results in the lengthening of the rigid rod chemical moiety, thus, resulting in the inducement of liquid crystallinity to the formed complex.

In the recent past, Frechet, Kato, and their research group [15–24] have activated the liquid crystal research through hydrogen bonding to set in to a new direction of research activity. The lower activation energies involved with the hydrogen bond interaction profoundly influence the thermal properties of liquid crystalline phases, viz., melting points, enthalpies, and thermal stability. Further, intermolecular hydrogen bond of complementary type in liquid crystalline materials is known to monitor the phase stability by the proper selection of interacting individual components. Hydrogen bond in liquid crystals can be realized by the interaction between a proton donor moiety and a proton acceptor moiety that are referred to as complimentary bonds. Complementary-type HBLCs can also be materialized [25–28] by the hydrogen bond interaction of two organic acids, such that each of them possessing an acid moiety bears a hydroxyl group considered as a proton donor and a carbonyl group considered as a proton acceptor. In order to realize the liquid crystallinity, it is considered as a sufficient condition that at least one of the moieties should be inherently [8,10] mesogenic. Most of the reported cases [9,25,28] of HBLCs deal with both the moieties being mesogenic, however, HBLCs made up of two moieties that are inherently non-mesogenic [29–31] are also reported. In summation, hydrogen bond interaction can enhance the thermal stability of device relevant tilted phases and better their operating parameters.

Though various structures of HBLCs are exist, an HBLC that possesses carboxylic acids on either sides of the chemical structure with varying $(CH_2)_n$ group (where n varies from 3–12) in the middle of the structure is quite interesting and keen to investigate. To materialize such a family of mesogens, the present work is proposed with dicarboxylic acids, viz., adipic acid (AA) whose *n* value equals three. The length of the molecule (*l*) and the distance between the layers (*d*), *l*/*d* ratio variation to the alkyloxy carbon (nBAO) chain attached to the AA by means of intermolecular hydrogen bonding, lead to the inducement of new phases. The occurrence and abundance of traditional orthogonal and smectic phases are studied with respect to their transition temperatures, mesogenic thermal ranges, order of the phase transitions, etc., through polarizing optical microscopy (POM), differential scanning calorimetry (DSC), and dielectric studies.

2. Experimental

Optical textural observations were made with Nikon polarizing microscope equipped with Nikon digital Charge-Coupled Device (CCD) camera system with 5 mega pixels and 2560 × 1920 pixel resolutions. The liquid crystalline textures were analyzed and stored with the aid of ACT-2U imaging software system. The temperature control of the liquid crystal cell was equipped by Instec HCS402-STC 200 temperature controller (Instec, USA) to a temperature resolution of ± 0.1 °C. This unit was further interfaced to a computer by IEEE–STC 200 to control and monitor the temperature. The liquid crystal sample was filled by capillary action in its isotropic state into a commercially available (Instec, USA) polyamide buffed cell with 10 μm spacer. Optical extinction technique [32] was used for determination of tilt angle. Transition temperatures and corresponding enthalpy values were obtained by DSC (Shimadzu DSC-60, Kyoto, Japan). Fourier transform infrared spectroscopy (FTIR) spectra was recorded (ABB FTIR MB3000, Quebec, Canada) and analyzed with the MB3000 software. Dielectric studies were performed by impedance analyzer (Agilent 4192 A). The AA and p-n-alkyloxy benzoic acids (nBAO, where

n = 5–12) were supplied by Sigma Aldrich (Steinheim, Germany) and all the solvents were of high-performance liquid chromatography (HPLC) grade.

2.1. Synthesis of HBLC

The inter hydrogen-bonded complexes examined in the present study are prepared by mixing 1:2 molar ratio of AA with various alkyloxy benzoic acids in excess dimethyl formamide (DMF) and reprecipitating after the evaporation as described in the reported literature [15–17]. The molecular structure of the present HBLC is shown below:

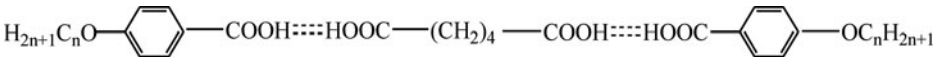

3. Results and Discussion

AA+nBAO hydrogen-bonded complexes isolated under the present investigation are white crystalline solids and are stable at room temperature (30°C). They are insoluble in water and sparingly soluble in common organic solvents, such as methanol, ethanol, benzene, and dichloro methane. However, they show a high degree of solubility in coordinating solvents like dimethyl sulfoxide (DMSO), DMF, and pyridine. They melt at specific temperatures below ~118.2°C (Table 1) and show high thermal and chemical stability when subjected to repeated thermal scans performed during POM and DSC studies.

3.1. Phase Identification

The observed phase variants, transition temperatures, and corresponding enthalpy values obtained by DSC in the cooling and heating cycles for the AA + nBAO complexes are presented in Table 1. The transition temperatures and phases observed are in concurrence with POM data.

3.2. Phase Polymorphism of AA+nBAO Homologous Series

The mesogens of the AA with nBAO (where n = 5–12) designated as AA+nBAO homologous series are found to exhibit characteristic textures [33], viz., nematic (N) (four brush texture, Plate 1), smectic C (broken focal conic texture, Plate 2), and smectic F (chequered board texture, Plate 3), respectively. The general phase sequence of various homologues of AA+nBAO series in cooling and heating runs can be shown as

Isotropic $\leftrightarrow$ N $\leftrightarrow$ SmC $\rightarrow$ SmF $\rightarrow$ Crystal (AA + 12BAO, AA + 9BAO)

Isotropic $\leftrightarrow$ N $\leftrightarrow$ SmC $\rightarrow$ SmF $\rightarrow$ Crystal (AA + 11BAO, AA + 10BAO)

Isotropic $\leftrightarrow$ N $\rightarrow$ SmF $\rightarrow$ Crystal (AA + 8BAO)

Isotropic $\leftrightarrow$ N $\rightarrow$ SmF $\rightarrow$ Crystal (AA + 7BAO, AA + 6BAO, AA + 5BAO)

Monotropic and enantiotropic transitions are depicted as single and double arrows, respectively.

Table 1. Transition temperatures obtained by different techniques for AA+nBAO homologous series. Enthalpy values (J/g) are given in parenthesis

Complex	Phase variance	Study	Crystal to melt	N	C	F	Crystal
AA+12BAO	NCF	DSC (h)	95.2 (76.97)	#	124.1 (2.6)	#	
		DSC (c)		120.0 (merged with C)	115.9 (32.1)	81.8 (22.95)	64.7 (9.29)
		POM (c)		116.5	120.5	82.1	64.9
AA+11BAO	NCF	DSC (h)	97.1 (88.31)	119.9 (4.22)	#	#	
		DSC (c)		117.6 (2.20)	115.4 (39.27)	80.4 (23.75)	70.3 (15.11)
		POM (c)		118.1	115.9	80.7	70.5
AA+10BAO	NCF	DSC (h)	88.9 (6.37)	126.6 (11.94)	#	#	
		DSC (c)		124.9 (8.98)	94.7 (0.95)	82.1 (22.95)	63.8 (12.02)
		POM (c)		125.4	95.1	82.4	64.0
AA+9BAO	NCF	DSC (h)	94.0 (64.57)	#	106.3 (2.16)	#	
		DSC (c)		117.6 (0.51)	102.0 (1.61)	84.6 (19.02)	63.2 (42.44)
		POM (c)		113.9	102.5	84.9	63.4
AA+8BAO	NF	DSC (h)	98.6 (38.74)	#		#	
		DSC (c)		136.9 (2.47)		117.5 (37.03)	89.7 (34.14)
		POM (c)		137.4		117.9	90.2
AA+7BAO	NF	DSC (h)	92.3 (80.86)	127.8 (23.73)		#	
		DSC (c)		122.8 (3.87)		83.4 (37.08)	72.8 (19.65)
		POM (c)		123.4		83.7	73.0
AA+6BAO	NF	DSC (h)	100.8 (43.94)	129.4 (45.37)		#	
		DSC (c)		127.1 (4.90)		115.8 (55.45)	93.3 (41.54)
		POM (c)		127.5		116.1	93.5
AA+5BAO	NF	DSC (h)	118.2 (58.15)	126.8 (24.50)		#	
		DSC (c)		124.7 (4.93)		113.9 (18.28)	109.8 (57.45)
		POM (c)		125.1		114.2	110

Note: #: monotropic transition, (c): cooling run, (h): heating run.

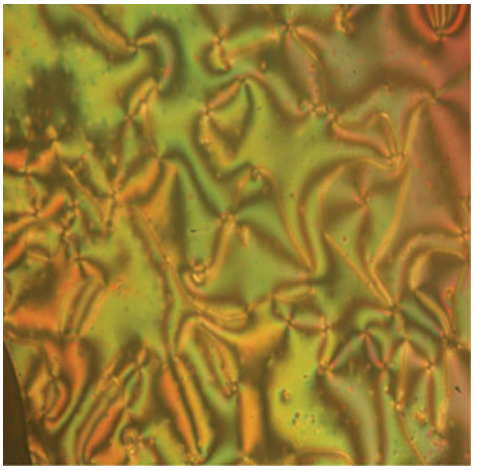

Plate 1. Nematic texture observed in AA+7BAO.

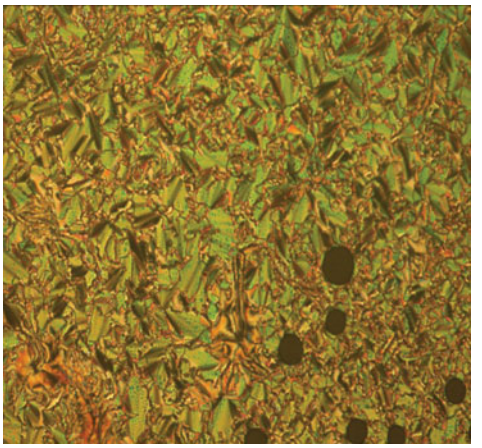

Plate 2. Broken focal conic texture of smectic C observed in AA+10BAO.

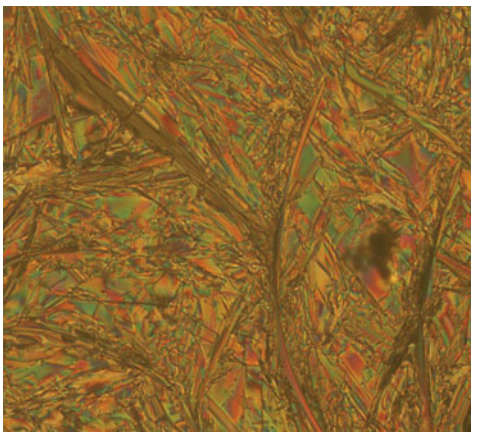

Plate 3. Chequered board texture of smectic F observed in AA+11BAO.

3.3. Fourier Transform Infrared Spectroscopy

IR spectra for all the eight homologues of AA+nBAO series have been recorded in the solid state (KBr) at room temperature. As a representative case, FTIR spectrum of AA+10BAO complex is shown in Figure 1 and is discussed elaborately. It is reported [34,35] that in the alkyloxy benzoic acids, carboxylic acid exists in monomeric form and the stretching vibration of C=O is observed at 1760 cm^{-1}. Further it is known [36] that when a hydrogen bond is formed between carboxylic acids, it results in lowering of the carbonyl frequency that has been detected in the present hydrogen-bonded complexes. A noteworthy feature in the spectrum of the AA+10BAO is the appearance of sharp peak at 1672 cm^{-1}, which clearly suggests the dimer formation in particular the carbonyl group vibration [35–37]. A carboxylic acid existing in monomeric form in dilute solution absorbs at about 1760 cm^{-1} because of the electron-withdrawing effect. However, acids in concentration solution or in solid state tend to dimerize through hydrogen bonding. It is reported [35,36] that this dimerization weakens the C=O bond and lowers the stretching force constant K, resulting in a lowering of the carbonyl frequency of saturated acids to ∼1710 cm^{-1}. This result concurs with the reported data of Kato et al. [34]. Hence, in the present complexes the formation of H bonding is established by FTIR. A similar trend of result is followed in all the other synthesized hydrogen-bonded complexes.

3.4. DSC Studies

DSC thermograms are obtained in heating and cooling cycles of the sample. The sample is crimped in an aluminum pan and heated at a scan rate of 10°C min^{-1} in nitrogen environment and held at its isotropic temperature for 1 min to attain thermal stability. The cooling run is also performed with the same scan rate of 10°C min^{-1}. A program is written in the DSC software TA 60 specifying the scan rate, hold temperature, and hold time. Respective equilibrium transition temperature and corresponding enthalpy values for each of the mesogens are recorded using the software of the DSC. DSC results are in conformity with the POM data. As a representative case, DSC thermogram obtained for AA+9BAO complex depicted in Figure 2 is discussed. From Figure 2 and Table 1, it can be inferred

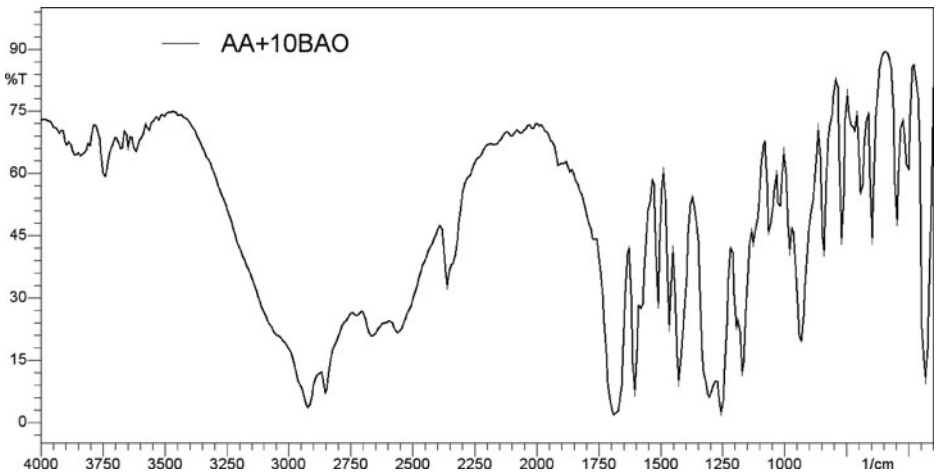

Figure 1. FTIR spectra of AA+10BAO complex.

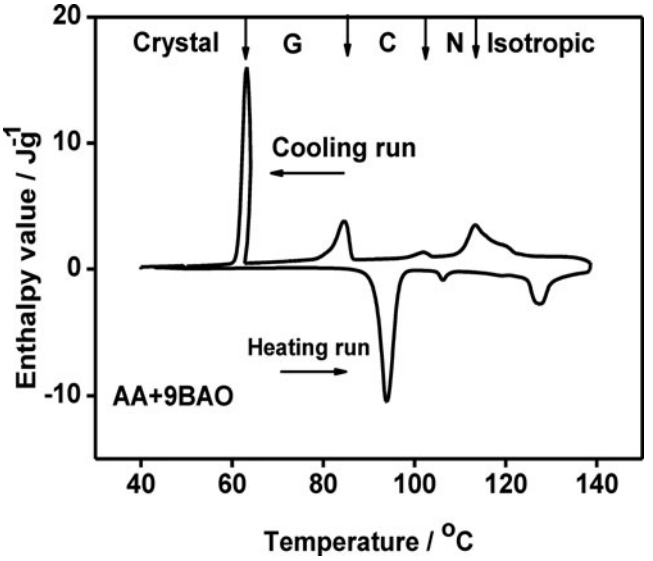

Figure 2. DSC thermogram of AA+9BAO complex.

that DSC heating run exhibits two endothermic peaks at 94.0°C and 106.3°C with enthalpy values of 64.57 J g^{-1} and 2.16 J g^{-1}, respectively. These two peaks correspond to the crystal to melt and smectic C to nematic phase transitions. The cooling run exhibits four peaks at 117.6°C, 102.2°C, 84.6°C, and 63.2°C with enthalpy values of 0.51 J g^{-1}, 1.61 J g^{-1}, 19.02 J g^{-1}, and 42.44 J g^{-1}, respectively. These exothermic peaks correspond to isotropic to nematic, nematic to smectic C, smectic C to smectic F, and smectic F to crystal phases, respectively. Thus, all the transitions are enantiotropic in cooling run, while in the heating run nematic to smectic C and smectic F to smectic C are observed to monotropic.

3.5. Phase Diagram

The phase diagram is composed of three phases, viz., nematic, smectic C, and smectic F. The salient features of the phase diagram as depicted in Figure 3 are detailed below:

(a) In all the eight hydrogen-bonded complexes, nematic and smectic F phases are observed with different thermal ranges.
(b) Odd–even effect is evinced at isotropic to nematic phase transition temperature in the present hydrogen bonded series.
(c) Smectic C is induced at nonyloxy carbon number quenching the nematic thermal range.
(d) Pentyloxy carbon number has the least mesogenic thermal range (14.9°C), while decyloxy carbon number possesses the highest (61.1°C), hence a threefold increase is noticed (Figure 4).
(e) Nematic thermal range is largest in heptyloxy, while dodecyloxy and octyloxy carbon numbers exhibit large thermal ranges of smectic C and smectic F, respectively.
(f) In general, in the homologous series, all the transitions, viz., isotropic to nematic, nematic to smectic C, smectic C to smectic F, and smectic F to crystal are observed to be first order.

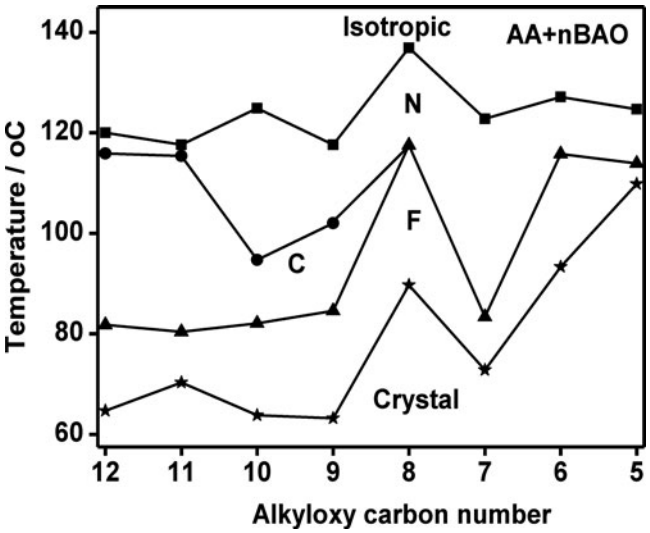

Figure 3. Phase diagram of AA+nBAO homologous series.

(g) The temperatures at which the individual mesogen attained crystallinity are dependent on the alkyloxy carbon number. In other words, as the carbon number is increased the crystallinity temperature decreased with an exception of octyloxy and undecyloxy benzoic acids.

3.5.1. Mesogenic Range. The mesogenic range, viz., the thermal span from isotropic to crystal in the cooling run is calculated for individual HBLC. Based upon the molecular

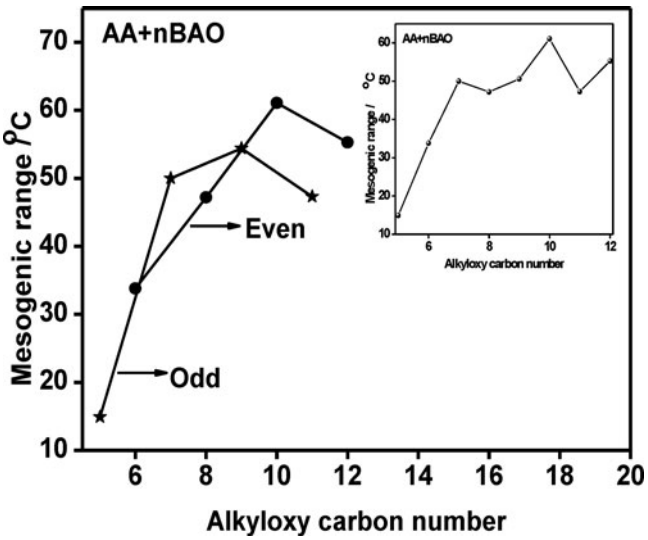

Figure 4. Mesogenic thermal range exhibited by odd and even complexes of AA+nBAO. Insert: Mesogenic thermal range exhibited by AA+nBAO homologous series.

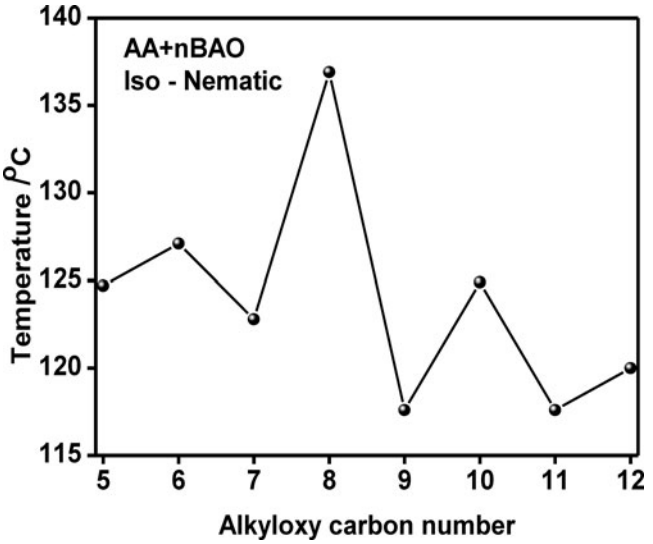

Figure 5. Odd–even effect at isotropic to nematic transition temperatures.

structures synthesized, the following points are observed with respect to observed phase transitions and liquid crystalline stabilities.

(i) For a mesophase to be obtained in any synthesized complex, it is necessary that the terminal chemical groups of the molecules contain permanent dipoles and dispersion forces.
(ii) Carboxylic acid is one among the terminal groups exhibiting dipole in nature. Since this AA+nBAO series possesses good thermal mesogenic range.
(iii) In the lower members of the homologous series, nematic is predominant, while in the higher members of the homologous series, the smectic phases encroached by suppressing the nematic phase that is due to increased dispersion forces and increased shielding of terminal dipolar attraction of terminal groups thus elevating the mesogenic range.
(iv) The above argument is supported by the data obtained from Figure 4, explaining the thermal mesogenic range exhibited by odd and even complexes, respectively.
(v) The mesogenic range of all the homologues is shown in the insert of Figure 4.

3.5.2. Odd–Even Effect. Odd–even effect is predominantly noticed in the present homologous series. A plot is constructed with the transition temperatures corresponding to the isotropic to nematic phase on the *y*-axis and the alkyloxy carbon number on the *x*-axis. Figure 5 depicts such variation of transition temperatures with carbon numbers in AA+nBAO homologous series. From Figure 5, it can be observed that the magnitudes of the transition temperatures corresponding to the even homologous carbon number (AA+6BAO, AA+8BAO, AA+10BAO, and AA+12BAO) exhibit one type of behavior, while their odd counter parts (AA+5BAO, AA+7BAO, AA+9BAO, and AA+11BAO) show a different increment. In the literature, such behavior has been reported [38, 39] and is referred to as odd–even effect.

The origin of the odd–even effect [38–42] can be understood from the consideration of the molecular structure. In the even numbers of the series, the disposition of the end

Table 2. Thermal stability factor obtained for various phases of AA+nBAO complexes

Complex	N	C	F
AA+5BAO	1288.44	—	458.59
AA+6BAO	1372.39	—	2352.38
AA+7BAO	4062.14	—	827.86
AA+8BAO	2467.68	—	2880.08
AA+9BAO	1712.88	1623.42	1581.46
AA+10BAO	3315.96	1113.84	1334.99
AA+11BAO	256.3	3426.5	761.04
AA+12BAO	483.60	3370.79	1252.58

group is such as to enhance the molecular anisotropy and hence molecular order, whereas in the odd number it has the opposite effect. As the chain length increases, their flexibility increases and the odd–even effect becomes less pronounced. The results of the odd–even effect observed in the present series are in accordance with the quantitative calculations proposed by Marcelja [38,41].

It may be noted that the present linear alternate intermolecular hydrogen-bonded liquid crystalline molecule is composed of a rigid aromatic ring and a flexible hydrogen-bonding part. The rigid core length varies with increment in the alkyloxy benzoic acid carbon chain. The rich liquid crystalline phase polymorphism with increment of alkyloxy carbon chain length is thus attributed to this part of the chemical structure. Moreover, the length (l) of the total HBLC varies with the alkyloxy carbon chain length while the width (d) remains constant. Thus, the altering of l/d ratio triggers the phase variance in the homologous series, which in turn influences the phase transition temperatures and the corresponding enthalpy values. Hence, the rigid cores and l/d ratio plays a vital role in establishing the pronounced odd–even effect as evinced in the present homologous series.

3.6. Phase Thermal Stability

It is reported [43,44] that when the liquid crystal molecules have two end chains, the phase transition temperatures are higher for the systems with equal chain length (symmetric). In a symmetric system, the end chains affect the phase transition temperatures as well as the temperature ranges of various phases. The molecular weights of terminal chain could be considered as the measure of balancing and if they are nearly equal, the system is balanced. In other words, the system is symmetric about its molecular short axis.

Phase stability is one of the important parameters that govern the utility of the mesogen. Phase stability of nematic is discussed. The term nematic phase stability can be attributed to isotropic to nematic transition temperature as well to the temperature range of nematic phase. It is reasonable to consider both the above factors and define a parameter called stability factor (S). The stability factor for nematic, S_N, is given by

$$S_N = T_{mid} * \Delta T_N,$$

where T_{mid} is the mid nematic temperature and ΔT_N is the nematic thermal range. In this manner, the thermal stability of smectic C and smectic F exhibited by different homologues

are calculated and tabulated in Table 2. From Table 2, it can be seen that the even and odd complexes show similar zig-zag trends in smectic C phase.

3.7. Optical Tilt Angle Studies

Optical tilt angle is deduced by optical extinction method [32] in smectic C phase for all the members of AA+nBAO homologous series. Figure 6 depicts such variation of optical tilt angle with temperature for AA+nBAO (where $n = 9$–12) series. The theoretical fit obtained is denoted by the solid line. Further, the tilt angle increases with decreasing temperature. For complexes AA+9BAO, AA+10BAO, AA+11BAO, and AA+12BAO, the maximum magnitudes of tilt angle are observed to 17°, 13.40°, 11.36°, and 13.12°, respectively. These large magnitudes of the tilt angle are owed to the direction of the soft covalent hydrogen bond interaction, which spreads along molecular long axis with finite inclination. Tilt angle is a primary order parameter [32] and the temperature variation is estimated by fitting the observed data of θ (T) to the relation

$$\theta(T)\alpha(T_C - T)^{\beta} \tag{1}$$

The critical exponent β value estimated by fitting the data of θ (T) to Equation (1) is found to be 0.50 to agree with the Mean Field prediction [39,45].

3.8. Dielectric Studies

Temperature variation of permittivity and dielectric loss has been discussed for two complexes, viz., AA+12BAO and AA+10BAO at 100 kHz. The sample is filled in its isotropic state into the commercially available 10 μ cell with an active area of 1 mm^2. Silver wires are drawn as leads from the cell and it is calibrated for temperature and frequency. The

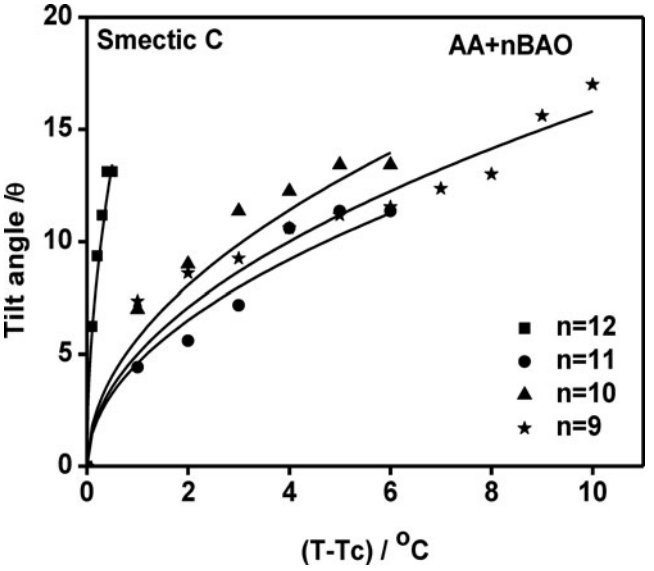

Figure 6. Temperature variation of tilt angle in smectic C phase of AA+nBAO ($n = 9$–12).

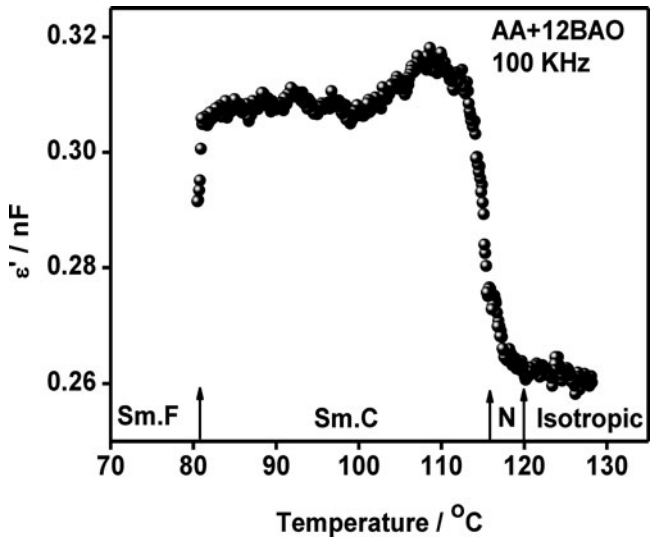

Figure 7. Temperature variation of capacitance at 100 kHz identifying various mesogens of AA+12BAO complex.

leads capacitance is calculated by a known substance (benzene). The samples are scanned in a frequency range of 5 Hz to 13 MHz with an oscillating voltage of 1.1 V.

3.8.1. Dielectric Spectrum of AA+12BAO. The variation of permittivity with temperature for the sample AA+12BAO is depicted in Figure 7. Simultaneous textural observations are undertaken for the identification of the phase. The sample is taken to isotropic state and hold for 10 min for attaining thermal stability. The sample is slowly cooled with a scan rate of 0.1°C min^{-1} programed by INSTEC temperature controller. In the thermal span of 125°C–120°C, in the isotropic state a linear variation of capacitance is observed. As the temperature is decreased at 119.9°C, the onset of the nematic phase is observed as nematic droplets and the phase transition of isotropic to nematic is seen as a kink in the dielectric profile. The nematic droplets coalesce to form a four brush texture (Plate 1). In the entire thermal span of nematic (119.9°C–116°C), a slight increase in the capacitance is noticed manifesting the stabilization of the nematic phase. The onset of smectic C is identified with the broken focal conic texture (Plate 2) and an instant steep increase in the capacitance is noticed. In the entire thermal span of smectic C (115.9°C–81.8°C), unaltered magnitude of the capacitance with temperature is noticed indicating the stabilization of the smectic C phase. Minute variation in the capacitance is attributed to the parachromatic changes in the broken focal conic texture. The change of color of the texture is because of varying refractive index in the phase. At 81.7°C, a steep fall in the capacitance is noticed, which is attributed to the smectic C to smectic F phase transition. The texture changed from broken focal conic to chequered board (Plate 3) indicating the first-order transition.

Similar changes are observed in the dielectric loss profile indicating the various phase transitions. The phase transition temperatures obtained by dielectric studies are in concurrence with POM and DSC results.

3.8.2. Dielectric Spectrum of AA+10BAO. In continuation with the investigation of the dielectric spectra of AA+12BAO, a similar examination is carried out for AA+10BAO

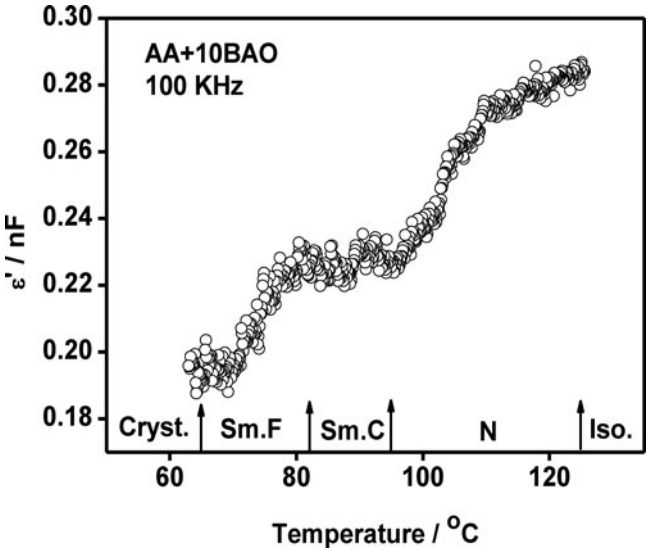

Figure 8. Temperature variation of capacitance at 100 kHz identifying various mesogens of AA+10BAO complex.

complex to analyze the temperature response of capacitance profile in its various phases. Capacitance variation with temperature is measured in the entire thermal range of the mesogenic complex (125.6°C–63°C) and is depicted in Figure 8.

In the thermal span between 125.6°C and 125°C, an unaltered magnitude of the capacitance is observed in its isotropic state. A linear proportional change of the capacitance profile in the entire thermal range of nematic (124.9°C–94.7°C) phase (four brushes, Plate 1) is observed indicating the stabilization of the phase. Simultaneous textural observations are made through POM to confirm the phase transition.

A sudden increase in the magnitude of the capacitance observed as a kink in Figure 8 contributes to the inducement of smectic C phase (broken focal conic texture, Plate 2) at a temperature of 94.7°C, which prevails till it reaches 82.2°C. At 82.1°C, a subtle deviation in the magnitude of capacitance is noticed clearly depicting the onset of smectic F phase (chequered board, Plate 3), which is a first-order phase transition as it is further confirmed from its enthalpy value obtained from its DSC thermogram. On further decrement of the temperature, the capacitance attains a constant magnitude at 63.8°C indicating the formation of crystal. The legitimacy of variation in capacitance is also proved by the data obtained from DSC and POM studies. Similar changes are observed in the dielectric loss profile indicating the various phase transitions.

3.8.3. Dielectric Relaxations. Dielectric dispersion, i.e., frequency variation of dielectric loss exhibited by AA+9BAO, AA+10BAO, and AA+11BAO are studied at different temperatures in smectic C phase in the frequency range of 5 Hz to 13 MHz. An impedance analyzer (Agilent 4192A LF) is operated with $1.1V_{P\text{-}P}$ oscillating signal with zero bias field. Relative permittivity $\varepsilon'_r(\omega)$ and dielectric loss $\varepsilon''(\omega)$ are calculated by the following equations:

$$*\varepsilon'_r(\omega) = \varepsilon'_r(\omega) - j\varepsilon''(\omega)$$

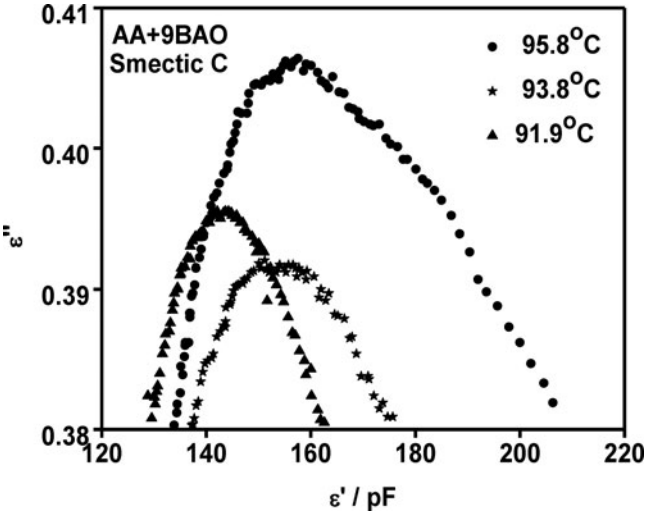

Figure 9. Dielectric dispersion curves in smectic C phase of AA+9BAO complex.

$$\varepsilon'_{\mathrm{r}}(\omega) = [C_{\mathrm{LC}} - C_{\mathrm{leads}}]/[C_{\mathrm{empty}} - C_{\mathrm{leads}}]$$
$$\varepsilon'_{\mathrm{r}}(\omega) = \mathrm{Tan}\delta(\omega)^{*}\varepsilon_{r}(\omega)$$

To detect the possible relaxation in the AA+nBAO complexes, the mesogens are scanned in the frequency range of 5 Hz to 13 MHz at different temperatures in the smectic C phase of the corresponding complex. The relaxation frequency (f_{r}) increases with lowering temperature, which is suggestive of an Arrhenius behavior [46–48] as it reflects the collective response. Further, the magnitude of the dielectric loss is shifted and is not suppressed by the temperature. The slope of the log of relaxation frequency to inverse of temperature, referred to as Arrhenius plot, gives the activation energy of the phase.

The corresponding dispersion curves and Arrhenius plots for all the complexes studied are illustrated in Figures 9–12 and they appear to be asymmetric about $\varepsilon''_{\mathrm{max}}$. Such an asymmetric non-Debbie's type of off-centered dispersion is studied by Cole–Davidson theory given by

$$\varepsilon''(\omega) = \{\varepsilon_{\infty} - [(\Delta\varepsilon)]/[1 + (j\omega\tau)^{1-\alpha}]\},$$

where $\Delta\varepsilon = (\varepsilon_{\mathrm{o}} - \varepsilon_{\infty})$ is the dielectric increment (strength), $\omega = 2\pi f$ (where f is the frequency of AC signal), ω is the relaxation time, i.e., $1/f_{\mathrm{r}}$, and α is the distribution parameter (or degrees of freedom) to estimate the influence of environment of dipoles and its fixation in the molecular frame during the reorientation to the field.

3.8.4. Dielectric Relaxations in AA+9BAO. The dielectric relaxations in AA+9BAO complex have been investigated in the entire thermal span of smectic C phase (102°C–84.6°C) at five temperatures, viz., 99.7 °C, 97.7°C, 95.8°C, 93.8°C, and 91.9°C, respectively.

The shift of the relaxation frequency to higher side with decrease in temperature can be noticed from Figue 9. The relaxation frequency at 99.7°C is 1125 kHz with an ε'' value of 0.4832, it has shifted to 2225 kHz as the temperature has decreased to 91.9°C with an ε'' value of 0.3955. Thus in this complex, the relaxation frequency in smectic C phase is inversely proportional to the temperature. From the above data plots, Arrhenius plot

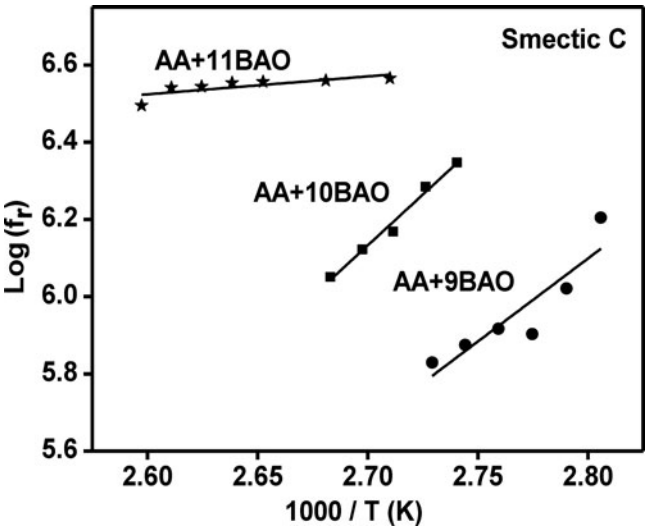

Figure 10. Arrhenius plot of AA+9BAO, AA+10BAO, and AA+11BAO complexes.

(Figure 10) is constructed and the activation energy is estimated to be 5.267 eV. The values of relaxation frequency and corresponding temperature and activation energy are listed in Table 3.

3.8.5. Dielectric Relaxations in AA+10BAO. The dielectric relaxations in AA+10BAO complex have been investigated in the entire thermal span of smectic C phase

Table 3. Values of relaxation frequency and corresponding temperature along with activation energy for AA+nBAO ($n = 9$, 10, and 11) complexes in smectic C phase

Complex	T (°C)	Frequency (kHz)	ε''_{max}	Activation energy (eV)
AA+9BAO	99.7	1125	0.4832	5.267
	97.7	1325	0.4620	
	95.8	1475	0.4064	
	93.8	1925	0.3955	
	91.9	2225	0.3930	
AA+10BAO	93.4	675	0.4740	4.302
	91.4	750	0.4693	
	89.4	825	0.4249	
	87.4	800	0.4255	
	85.4	1050	0.4277	
	83.4	1600	0.4012	
AA+11BAO	110	3475	0.4787	0.466
	108	3500	0.4816	
	106	3575	0.4820	
	104	3600	0.4827	
	100	3625	0.4829	
	96	3675	0.4849	

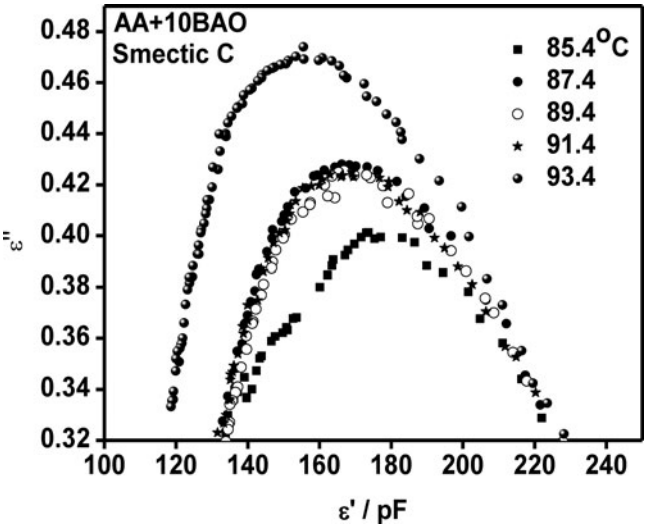

Figure 11. Dielectric dispersion curves in smectic C phase of AA+10BAO complex.

(94.7°C–82.1°C) at six temperatures, viz., 93.4 °C, 91.4°C, 89.4°C, 87.4°C, 85.4°C, and 83.4°C, respectively.

The shift of the relaxation frequency to higher side with decrease in temperature can be noticed from Figure 11. The relaxation frequency at 93.4°C is 675 kHz with an ε'' value of 0.4012, it has shifted to 1600 kHz as the temperature has decreased to 83.4°C with an ε'' value of 0.4693. Thus in this complex, the relaxation frequency in smectic C phase is inversely proportional to the temperature. From the above data plots, Arrhenius plot (Figure 10) is constructed and the activation energy is estimated to be 4.302 eV. The values of relaxation frequency and corresponding temperature and activation energy are listed in Table 3.

3.8.6. Dielectric Relaxations in AA+11BAO. The dielectric relaxations in AA+11BAO complex have been investigated in the entire thermal span of smectic C phase (115.4°C–80.4°C) at six temperatures, viz., 110°C, 108°C, 106°C, 104°C, 100°C, and 96°C, respectively.

The shift of the relaxation frequency to higher side with decrease in temperature can be noticed from Figure 12. The relaxation frequency at 110°C is 3475 kHz with an ε'' value of 0.4787, it has shifted to 3675 kHz as the temperature has decreased to 96°C with an ε'' value of 0.4849. Thus in this complex, the relaxation frequency in smectic C phase is inversely proportional to the temperature. From the above data plots, Arrhenius plot (Figure 10) is constructed and the activation energy is estimated to be 0.466 eV. The values of relaxation frequency and corresponding temperature and activation energy are listed in Table 3.

3.8.7. Dielectric Hysteresis. The complex AA+9BAO exhibits nematic phase with a wide range as discussed in the above sections. The complex filled in the commercially available polyamide buffed cell of 10 μ spacer is slowly cooled at 0.1°C min^{-1} to 109°C from isotropic for proper alignment, which is the mid thermal range of nematic phase. It is subjected to external voltage derived from impedance analyzer at 100 kHz. The external field is slowly increased in steps of 0.1 V μ^{-1} and the resultant permittivity is plotted as

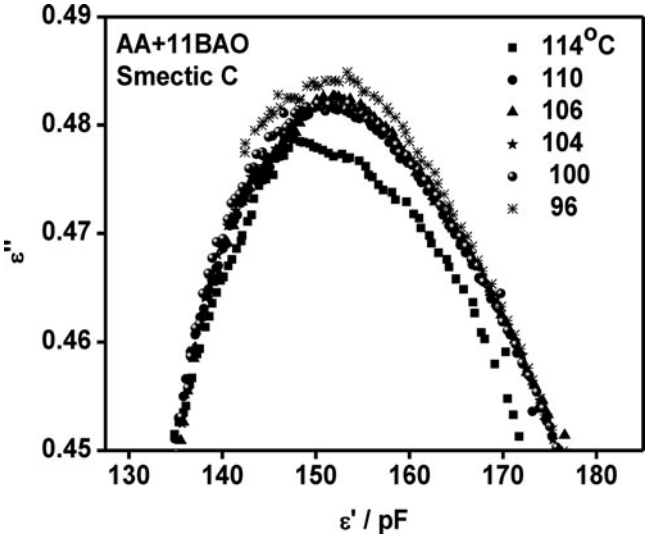

Figure 12. Dielectric dispersion curves in smectic C phase of AA+11BAO complex.

Figure 13. It is surprising to note in a non-ferroelectric complex the huge dielectric hysteresis and the considerable dielectric loop sandwiched in the two paths of the field. A similar dielectric hysteresis is reported [49] for 5CB in nematic phase, further this ferroelectric-type hysteresis effect clearly indicates the structural modification in the nematic matrix. Domain orientation in the presence of field is the major reason for the dielectric hysteresis. When the field is withdrawn, the domains fail to reorient to its original position resulting in the ferroelectric-type hysteresis. This can be used as memory effect, when a residual field is applied, the domains regain its original position.

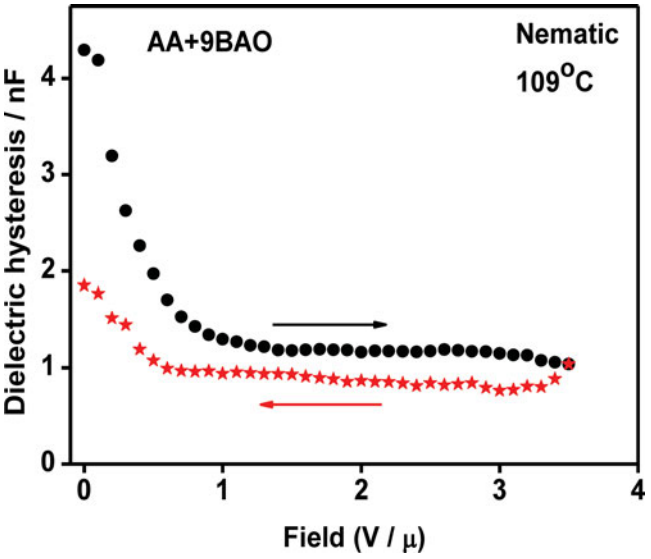

Figure 13. Dielectric hysteresis in nematic phase of AA+9BAO complex.

4. Conclusions

(i) A novel series of HBLC homologous series that varies in their alkyloxy carbon chain length is designed, synthesized, and characterized by various techniques.
(ii) Based on the molecular structure of the complexes formed, the thermal stability factor for various phases in AA+nBAO series have been estimated and explained.
(iii) Primary-order parameter and optical tilt angle are measured with respect to temperature in the smectic C phase, and the values obtained are fitted to a power-law equation describing the utility of the complexes in the display device applications.
(iv) Dielectric relaxation frequencies for different complexes in smectic phase are elucidated and the corresponding activation energy is determined to find out the anchoring energy of the molecules possessed in the corresponding phase.
(v) Dielectric hysteresis is measured in nematic phase with respect to the applied field and the results are discussed leading to the commercial viabilities.

Acknowledgments

The divine and graceful blessings of almighty Bannari Amman, the infrastructural support rendered by Bannari Amman Institute of Technology, and the financial support rendered by the Board of Research in Nuclear Sciences (BRNS) of Department of Atomic Energy (DAE), India (Sanction No. 2012/34/35/BRNS) are gratefully acknowledged.

References

[1] Brand, H. R., Cladis, P. E., & Pleiner, H. (1992). *Macromolecules*, *25*, 7223.
[2] Cook, A. G., Baumeister, U., & Tschierske, C. (2005). *J. Mater. Chem.*, *15*, 1708.
[3] Brienne, M. J., Gabard, J., Lehn, J. M., & Stibor, J. (1989). *J. Chem. Soc. Chem. Commun.*, 1868.
[4] Kato, T., Mizoshita, N., & Kanie, K. (2001). *Macromol. Rapid. Commun.*, *22*, 797.
[5] Paleos, C. M., & Tsiourvas, D. (1995). *Angew. Chem.*, *107*, 1839.
[6] Beginn, U. (2003). *Prog. Polym. Sci.*, *28*, 1049.
[7] Zimmerman, N., Moore, J. S., & Zimmerman, S. C. (1998). *Chem. Ind.*, *15*, 604.
[8] Pongali Sathya Prabu, N., & Madhu Mohan, M. L. N. (2011). *J. Mol. Str.*, *994*, 387.
[9] Pongali Sathya Prabu, N., & Madhu Mohan, M. L. N. (2013). *J. Mol. Liq.*, *182*, 79.
[10] Pongali Sathya Prabu, N., Vijayakumar, V. N., & Madhu Mohan, M. L. N. (2011). *Physica B.*, *406*, 1106.
[11] Gopunath, A. J., Chitravel, T., Kavitha, C., Pongali Sathya Prabu, N., & Madhu Mohan, M. L. N. (2013). *Mol. Cryst. Liq. Cryst.*, *547*, 19.
[12] Lehn, J. M. (1995). *Supramolecular Chemistry: Concept and Perspectives*, VCH: Weinheim.
[13] Fouquey, C., Lehn, J. M., & Mlevelut, A. (1990). *Adv. Mate.*, *2*, 254.
[14] Bradfield, E., & Jones, B. (1929). *J. Chem. Soc.*, 2661.
[15] Kato, T., & Frechet, J. M. J. (1995). *Macromol. Symp.*, *95*, 311.
[16] Kato, T., & Frechet, J. M. J. (1989). *J. Am. Chem. Soc.*, *111*, 8533.
[17] Kato, T., & Frechet, J. M. J. (1989). *Macromolecules*, *22*, 3818.
[18] Kato, T., Nakano, M., Moteki, T., Uryu, T., & Ujiie, S. (1995). *Macromolecules*, *28*, 8875.
[19] Kato, T. (1996). *Supra. Mol. Sci.*, *3*, 53.
[20] Kato, T., Wilson, P. G., Fujishima, A., & Frechet, J. M. J. (1990). *Chem. Lett.*, *19*, 2003.
[21] Kato, T., Fukumasa, M., & Frechet, J. M. J. (1995). *Chem. Mater.*, *7*, 368.
[22] Fukumasa, M., Kato, T., Uryu, T., & Frechet, J. M. J. (1993). *Chem. Lett.*, *22*, 65.
[23] Kato, T., Fujishima, A., & Frechet, J. M. J. (1990). *Chem. Lett.*, *19*, 919.
[24] Kato, T., Adachi, H., Fujishima, A., & Frechet, J. M. J. (1992). *Chem. Lett.*, *21*, 265.

[25] Pongali Sathya Prabu, N., & Madhu Mohan, M. L. N. (2013). *Phase Trans.*, *86*, 339.
[26] Pongali Sathya Prabu, N., Vijayakumar, V. N., & Madhu Mohan, M. L. N. (2011). *Mol. Cryst. Liq. Cryst.*, *548*, 142.
[27] Pongali Sathya Prabu, N., & Madhu Mohan, M. L. N. (2012). *Mol. Cryst. Liq. Cryst.*, *557*, 190.
[28] Kavitha, C., Pongali Sathya Prabu, N., & Madhu Mohan, M. L. N. (2012). *Phase Trans.*, *85*, 973.
[29] Kang, S. K., & Samulski, E. T. (2000). *Liq. Cryst.*, *27*, 371.
[30] Hentrich, F., Diele, S., & Tschierske, C. (1994). *Liq. Cryst.*, *17*, 827.
[31] Kobayashi, Y., & Mtsunage, Y. (1987). *Bull. Chem. Soc. Jpn.*, *60*, 3515.
[32] Noot, C., Perkins, S. P., & Coles, H. J. (2000). *Ferroelectrics*, *244*, 331.
[33] Gray, G. W., & Goodby, J. W. G. (1984). *Smectic Liquid Crystals: Textures and Structures*, Leonard Hill: London.
[34] Kato, T., Uryu, T., Kaneuchi, F., Jin, C., & Frechet, J. M. J. (1993). *Liq. Cryst.*, *14*, 1311.
[35] Pavia, D. L., Lampman, G. M., & Kriz. G. S. (2007). *Introduction to Spectroscopy*, Sanat Printers: Kundli, India.
[36] Nakamoto, K. (1978). *Infrared and Raman Spectra of Inorganic and Co-ordination Compounds*, Interscience: New York.
[37] Xu, J. (2006). *J. Mater. Chem.*, *16*, 3540.
[38] Marcelja, S. (1973). *Solid State Commun*., *13*, 759.
[39] Chandrasekhar, S. (1977). *Liquid Crystals*, Cambridge University Press: New York.
[40] Thoen, J., Cordoyiannis, G., & Glorieux, C. (2009). *Liq. Cryst.*, *36*, 669.
[41] Marcelja, S., (1974). *J. Chem. Phys.*, *60*, 3599.
[42] Senthil, S., Rameshbabu, K., & Wu, S. L. (2006). *J. Mol. Str.*, *783*, 215.
[43] Smith, G. W., & Gardlund, Z. G. (1973). *J. Chem. Phys.*, *59*, 3214.
[44] Osman, Z. (1976). *Naturforsh*, *31b*, 801.
[45] Stanley, H. E. (1971). *Introduction to Phase Transition and Critical Phenomena*, Clarendon Press: New York.
[46] Hills, N. E., Wanghan, W. E., Price, A. H., & Davies, M. (1969). *Dielectric Properties and Molecular Behavior*, Vannostrand: New York.
[47] Jonscher, A. H. (1983). *Dielectric Relaxation in Solids*, Chelsea Dielectric Press: London.
[48] Cole, R. H. (1941). *J. Chem. Phys.*, *9*, 341.
[49] Basu, R., & Iannacchione, G. (2008). *Appl. Phys. Lett.*, *93*, 183105.